tiousness from 3 days after infection until slaughter (for an average of eight infectious days).

12. The effective neighborhood size, n, in units of nearest neighbor farms, was estimated as

$$n = \int_0^\infty g(r)dr \Big/ \int_0^R g(r)dr$$

where R is given by the solution of

$$\int_0^R \kappa(r)dr = 1$$

The connectedness of the contact network is given by

$$\phi = \frac{1}{n^2} \int\int\int g(r)g(r')g(|\mathrm{r} - \mathrm{r}'|)/\kappa(|\mathrm{r} - \mathrm{r}'|)drdr'd\theta$$

where

$$|\mathrm{r} - \mathrm{r}'| = r^2 + r'^2 - 2rr'\cos(\theta)$$

13. S. C. Howard, C. A. Donnelly, *Res. Vet. Sci.* **69**, 189 (2000).
14. D. T. Haydon, M. E. J. Woolhouse, R. P. Kitching, *IMA J. Math. Appl. Med. Bio.* **14**, 1 (1997).
15. The population of farms was stratified into a susceptible class, S; sequential infection classes, I_i ($i = 1..M$); and a slaughtered/vaccinated class, D. Multiple infected classes were used to exactly reproduce the gamma distribution fits to the delay data shown in Fig. 2 and to represent different stages of infectiousness and diagnosis. The mixture model of the infection-to-report distribution was represented by overlapping sets of 30 classes (transit time = 0.26 days each, weight 0.82) and 4 classes (transit times = 3.73 days, weight 0.18). Two classes (transit times = 0.85 to 0.21 days, time-dependent) represented farms awaiting disease confirmation after report, and four classes (transit times = 0.82 to 0.38 days, time-dependent)—overlapping the previous two—represented farms awaiting culling after disease reporting. Infectiousness varies as a function of incubation stage, reaching significant levels after around 3.5 days and then continuing at a constant level until diagnosis, after which it remains constant until slaughter at a level r_I times greater than before reporting. The model is novel in tracking not only the numbers of farms in each infection state through time, but also the numbers of pairs of farms connected on the contact network used to represent spatially localized disease transmission. For conciseness and clarity, we only present those for a simpler model with only two infected classes: E (uninfectious) and I (infectious). Using $[X]$ to represent the mean number in state X, $[XY]$ to represent the mean number of pairs of type XY, and $[XYZ]$ to represent the mean number of triples, the dynamics can be represented by the following set of differential equations: $d[S]/dt = -(\tau + \mu + \omega)[SI] - p\beta[S][I]/N$, $d[E]/dt = p\beta[S][I]/N + \tau[SI] - \nu[E] - \mu[EI]$, $d[I]/dt = \nu[E] - s[I] - \mu[II]$, $d[SS]/dt = -2(\tau + \mu + \omega)[SSI] - 2p\beta[SS][I]/N$, $d[SE]/dt = \tau([SSI] - [ISE]) - \mu([SEI] + [ISE]) - \omega[ISE] + p\beta([SS] - [SE])[I]/N$, $d[SI]/dt = \nu[SE] - (\tau + \mu + \omega)([ISI] + [SI]) - p\beta[SI][I]/N$, $d[EE]/dt = \tau[ISE] - 2\mu[EEI] - 2\nu[EE] + 2p\beta[SE][I]/N$, $d[EI]/dt = \nu[EE] - \mu([EI]+[IEI]) - (\nu + \sigma)[EI] + p\beta[SI][I]/N$, $d[II]/dt = 2\nu[EI] - 2\sigma[II] - 2\mu([II] + [III])$. The numbers of triples are calculated with the closure approximation (*16*) $[XYZ] \approx (n - 1)[XY][YZ](1 - \phi + \phi\, N[YY]/n[X][Z])/n[Y]$, where n is the mean contact neighborhood size of a farm, ϕ is the proportion of triples in the network that are triangles, and N is the total number of farms [see (*12*)]. $\tau = (1 - p)\beta/n$ is the transmission rate across a contact, where β is the transmission coefficient of the virus, and p is the proportion of contacts that are long-range [see (*9*)], both of which are estimated separately before and after the movement ban. ν is the rate of transit from the uninfectious to the infectious class, and σ is the rate of transit from the infectious to the removed class. μ is the rate at which farms in the neighborhood of an infected farm are culled in ring culling, and ω is the rate at which farms are vaccinated in ring vaccination. It is assumed that vaccination has no effect on previously infected farms.
16. M. J. Keeling, *Proc. R. Soc. London B* **266**, 859 (1999).
17. Removal by culling of an infected herd and the removal of contiguous holdings of animals have different impacts on R_0 and the scale of the epidemic. The former acts directly to reduce R_0, whereas the latter serves to significantly reduce the overall scale of the epidemic by stopping second-generation transmission events [hence reducing the effective reproductive number (*10*)].
18. *Northumberland Report: The Report of the Committee of Inquiry on Food and Mouth Disease* (Her Majesty's Stationery Office, London, 1968).
19. June 2000 Agricultural and Horticultural Census, Ministry of Agriculture, Fisheries and Food, National Assembly for Wales Agriculture Department and Scottish Executive Rural Affairs Department; Crown copyright, 2001.
20. The rapid decline in case incidence seen after completion of the analysis presented in this paper has given new estimates of r_I significantly above 1, though more precise estimation awaits availability of detailed data on all slaughter schemes in operation since 30 March 2001.

21. We are extremely grateful for help in the provision of data and for invaluable advice from J. Wilesmith (Veterinary Laboratory Agency), D. Reynolds (Food Standards Agency and Ministry of Agriculture, Fisheries and Food), and D. Thompson (Ministry of Agriculture, Fisheries and Food) and to the many government epidemiologists and veterinary staff who collected the unique contact tracing data on FMD spread in the current epidemic. In addition, we thank D. King (Office of Science and Technology), B. Grenfell, M. Keeling, M. Woolhouse, and other members of the FMD Official Science Group for stimulating discussions; Sir Robert May and Sir David Cox for valuable advice and discussions; three anonymous referees for comments; and S. Dunstan, S. Riley, and H. Carabin for valuable assistance. N.M.F. thanks the Royal Society and the Howard Hughes Medical Institute for fellowship and research funding support. C.A.D. and R.M.A. thank the Wellcome Trust for research funding.

23 March 2001; accepted 10 April 2001
Published online 12 April 2001;
10.1126/science.1061020
Include this information when citing this paper.

Structural Mechanism for Statin Inhibition of HMG-CoA Reductase

Eva S. Istvan[1] and Johann Deisenhofer[1,2]*

HMG-CoA (3-hydroxy-3-methylglutaryl–coenzyme A) reductase (HMGR) catalyzes the committed step in cholesterol biosynthesis. Statins are HMGR inhibitors with inhibition constant values in the nanomolar range that effectively lower serum cholesterol levels and are widely prescribed in the treatment of hypercholesterolemia. We have determined structures of the catalytic portion of human HMGR complexed with six different statins. The statins occupy a portion of the binding site of HMG-CoA, thus blocking access of this substrate to the active site. Near the carboxyl terminus of HMGR, several catalytically relevant residues are disordered in the enzyme-statin complexes. If these residues were not flexible, they would sterically hinder statin binding.

Elevated cholesterol levels are a primary risk factor for coronary artery disease. This disease is a major problem in developed countries and currently affects 13 to 14 million adults in the United States alone. Dietary changes and drug therapy reduce serum cholesterol levels and dramatically decrease the risk of stroke and overall mortality (*1*). Inhibitors of HMGR, commonly referred to as statins, are effective and safe drugs that are widely prescribed in cholesterol-lowering therapy. In addition to lowering cholesterol, statins appear to have a number of additional effects, such as the nitric oxide–mediated promotion of new blood vessel growth (*2*), stimulation of bone formation (*3*), protection against oxidative modification of low-density lipoprotein, as well as anti-inflammatory effects and a reduction in C-reactive protein levels (*4*). All statins curtail cholesterol biosynthesis by inhibiting the committed step in the biosynthesis of isoprenoids and sterols (*5*). This step is the four-electron reductive deacylation of HMG-CoA to CoA and mevalonate. It is catalyzed by HMGR in a reaction that proceeds as follows

$$\text{(S)-HMG-CoA} + 2\text{NADPH} + 2\text{H}^+ \rightarrow \text{(R)-mevalonate} + 2\text{NADP}^+ + \text{CoASH}$$

where $NADP^+$ is the oxidized form of nicotinamide adenine dinucelotide, NADPH is the reduced form of $NADP^+$, and CoASH is the reduced form of CoA.

Several statins are available or in late-stage clinical development (Fig. 1). All share an HMG-like moiety, which may be present in an inactive lactone form. In vivo, these prodrugs are enzymatically hydrolyzed to their active hydroxy-acid forms (*5*). The statins

[1]Department of Biochemistry, [2]Howard Hughes Medical Institute, University of Texas Southwestern Medical Center at Dallas, TX 75390–9050, USA.

*To whom correspondence should be addressed. E-mail: Johann.Deisenhofer@UTSouthwestern.edu

share rigid, hydrophobic groups that are covalently linked to the HMG-like moiety. Lovastatin, pravastatin, and simvastatin resemble the substituted decalin-ring structure of compactin (also known as mevastatin). We classify this group of inhibitors as type 1 statins. Fluvastatin, cerivastatin, atorvastatin, and rosuvastatin (in development by AstraZeneca) are fully synthetic HMGR inhibitors with larger groups linked to the HMG-like moiety. We refer to these inhibitors as type 2 statins. The additional groups range in character from very hydrophobic (e.g., cerivastatin) to partly hydrophobic (e.g., rosuvastatin). All statins are competitive inhibitors of HMGR with respect to binding of the substrate HMG-CoA, but not with respect to binding of NADPH (*6*). The K_i (inhibition constant) values for the statin-enzyme complexes range between 0.1 to 2.3 nM (*5*), whereas the Michaelis constant, K_m, for HMG-CoA is 4 μM (*7*).

Although the structure of the catalytic portion of human HMGR in complex with substrates and with products has recently been elucidated (*8*, *9*), it yields little information concerning statin binding. The protein forms a tightly associated tetramer with bipartite active sites, in which neighboring monomers contribute residues to the active sites. The HMG-binding pocket is characterized by a loop (residues 682–694, referred to as "cis loop") (Fig. 2A). Because statins are competitive with respect to HMG-CoA, it appeared likely that their HMG-like moieties might bind to the HMG-binding portion of the enzyme active site. However, in this binding mode their bulky hydrophobic groups would clash with residues that compose the narrow pocket which accommodates the pantothenic acid moiety of CoA; thus, the mechanism of inhibition has remained unresolved.

To determine how statins prevent the binding of HMG-CoA, we solved six crystal structures of the catalytic portion of human HMGR bound to six different statin inhibitors at resolution limits of 2.3 Å or higher (Table 1) (*10*). For each structure, the bound inhibitors are well defined in the electron-density maps (Fig. 3). They extend into a narrow pocket where HMG is normally bound and are kinked at the O5-hydroxyl group of the HMG-like moiety, which replaces the thioester oxygen atom found in the HMG-CoA substrate. The hydrophobic-ring structures of the statins contact residues within helices Lα1 and Lα10 of the enzyme's large domain (Fig. 2B). No portion of the elongated NADP(H) binding site is occupied by statins. The structures presented here illustrate that statins inhibit HMGR by binding to the active site of the enzyme, thus sterically preventing substrate from binding. This agrees well with kinetic studies that indicate that statins competitively inhibit HMG-CoA but do not affect NADPH binding (*6*).

A comparison between substrate-bound and inhibitor-bound HMGR structures clearly illustrates rearrangement of the substrate-binding pocket to accommodate statin molecules (Fig. 2). The structures differ in the COOH-terminal 28 amino acids of the protein. In the electron-density maps of the statin-complex structures, residues COOH-terminal to Gly^{860} are missing. In the substrate-complex structure, these residues encompass part of helix Lα10 and all of helix Lα11, fold over the substrate, and participate in the formation of the narrow pantothenic acid–binding pocket (Fig. 2A). In the statin-bound structures, these residues are disordered, revealing a shallow hydrophobic groove that accommodates the hydrophobic moieties of the statins.

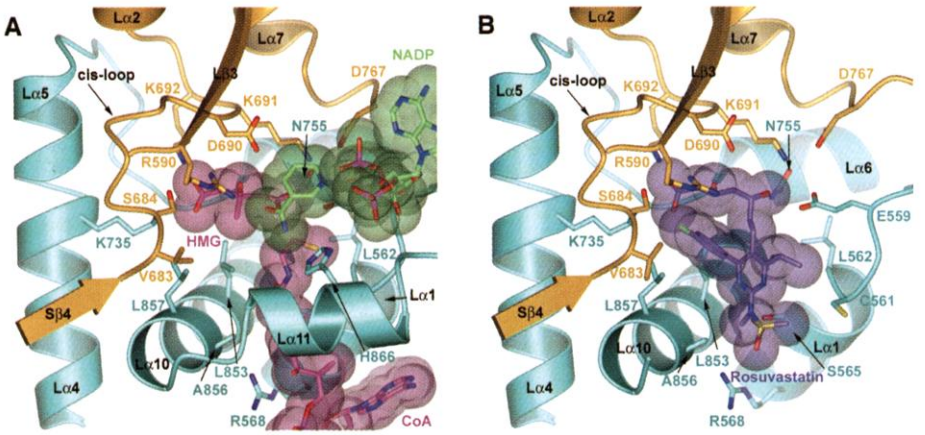

Fig. 2. Statins exploit the conformational flexibility of HMGR to create a hydrophobic binding pocket near the active site. (**A**) Active site of human HMGR in complex with HMG, CoA, and NADP. The active site is located at a monomer-monomer interface. One monomer is colored yellow, the other monomer is in blue. Selected side chains of residues that contact the substrates or the statin are shown in a ball-and-stick representation (*20*). Secondary structure elements are marked by black labels. HMG and CoA are colored in magenta; NADP is colored in green. To illustrate the molecular volume occupied by the substrates, transparent spheres with a radius of 1.6 Å are laid over the ball-and-stick representation of the substrates or the statin. (**B**) Binding of rosuvastatin to HMGR. Rosuvastatin is colored in purple; other colors and labels are as in (A). This figure and Figs. 3 and 4 were prepared with Bobscript (*22*), GLR (*23*), and POV-Ray (*24*).

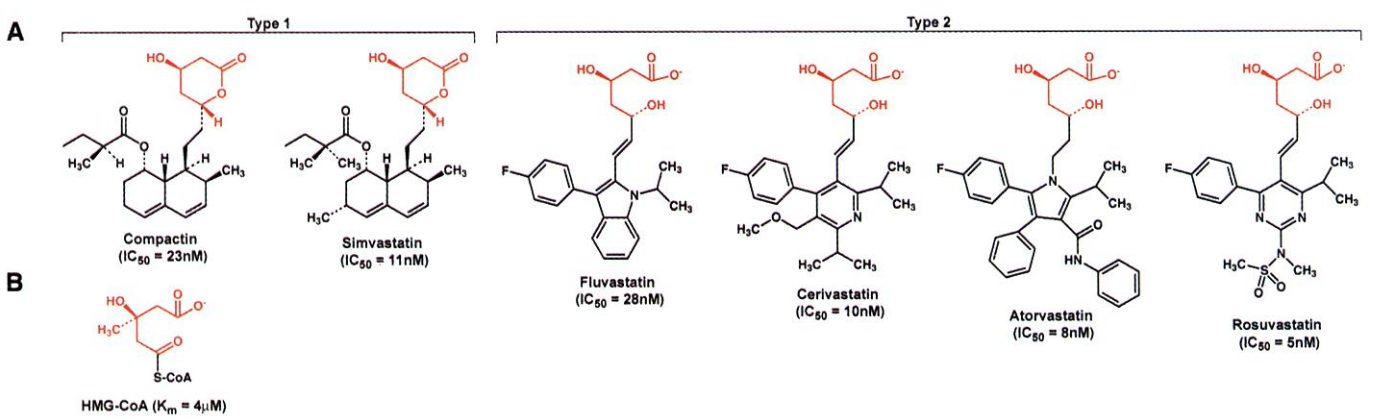

Fig. 1. Structural formulas of statin inhibitors and the enzyme substrate HMG-CoA. (**A**) Structure of several statin inhibitors. Compactin and simvastatin are examples of type 1 statins; not shown are the other type 1 statins, lovastatin and pravastatin. Fluvastatin, cerivastatin, atorvastatin, and rosuvastatin are type 2 statins. The HMG-like moiety that is conserved in all statins is colored in red. The IC_{50} (median inhibitory concentration) values of the statins are indicated (*21*). (**B**) Structure of HMG-CoA. The HMG-moiety is colored in red, and the K_m value of HMG-CoA is indicated (*7*).

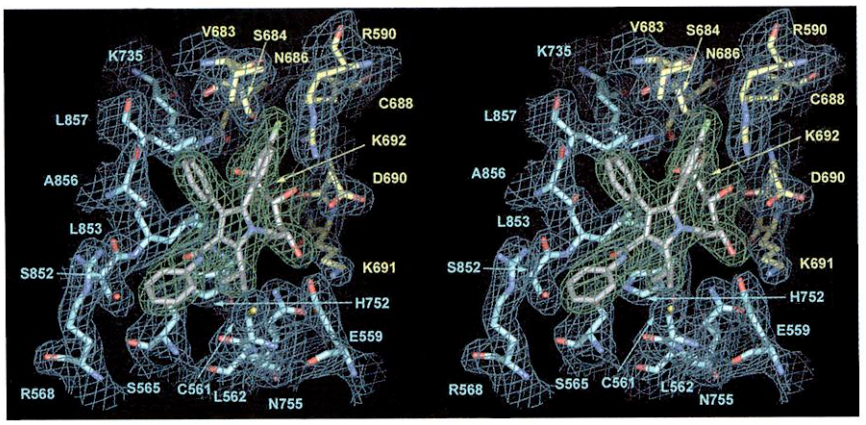

Fig. 3. Stereoview of the electron-density map of atorvastatin bound to the HMGR active site. This 2.2 Å simulated-annealing omit map, contoured at 1 σ, was calculated by omitting all atoms of the atorvastatin molecule shown, as well as protein atoms within 4.5 Å of the inhibitor. The electron density is overlaid on the final, refined model. The electron density covering atorvastatin is in green, whereas the electron density covering the protein is in blue. Carbon atoms of one of the two protein monomers are colored yellow, those of the neighboring monomer are in blue, and those of atorvastatin are in gray. In all molecules oxygen atoms are red, nitrogen atoms are blue, sulfur atoms are yellow, and the fluorine atoms are green.

Although the structural changes in the complexes with statin had not been predicted, the COOH-terminal residues of HMGR are known to be a mobile element in this protein. In structures of the human enzyme in complex with HMG-CoA alone, helix Lα11 was partially disordered (*8*). Similarly, in structures of a bacterial homolog of HMGR from *Pseudomonas mevalonii*, a larger COOH-terminal domain that is not present in the human protein is disordered when no substrates are present (*11*) but ordered in the ternary complex (*12*). It appears that the innate flexibility of the COOH-terminal region of HMGR is fortuitously exploited by statins to create a binding site for the inhibitor molecules.

How is the specificity and tight binding of statin inhibitors achieved? The HMG-moieties of the statins occupy the enzyme active site of HMGR. The orientation and bonding interactions of the HMG moieties of the inhibitors clearly resemble those of the sub-

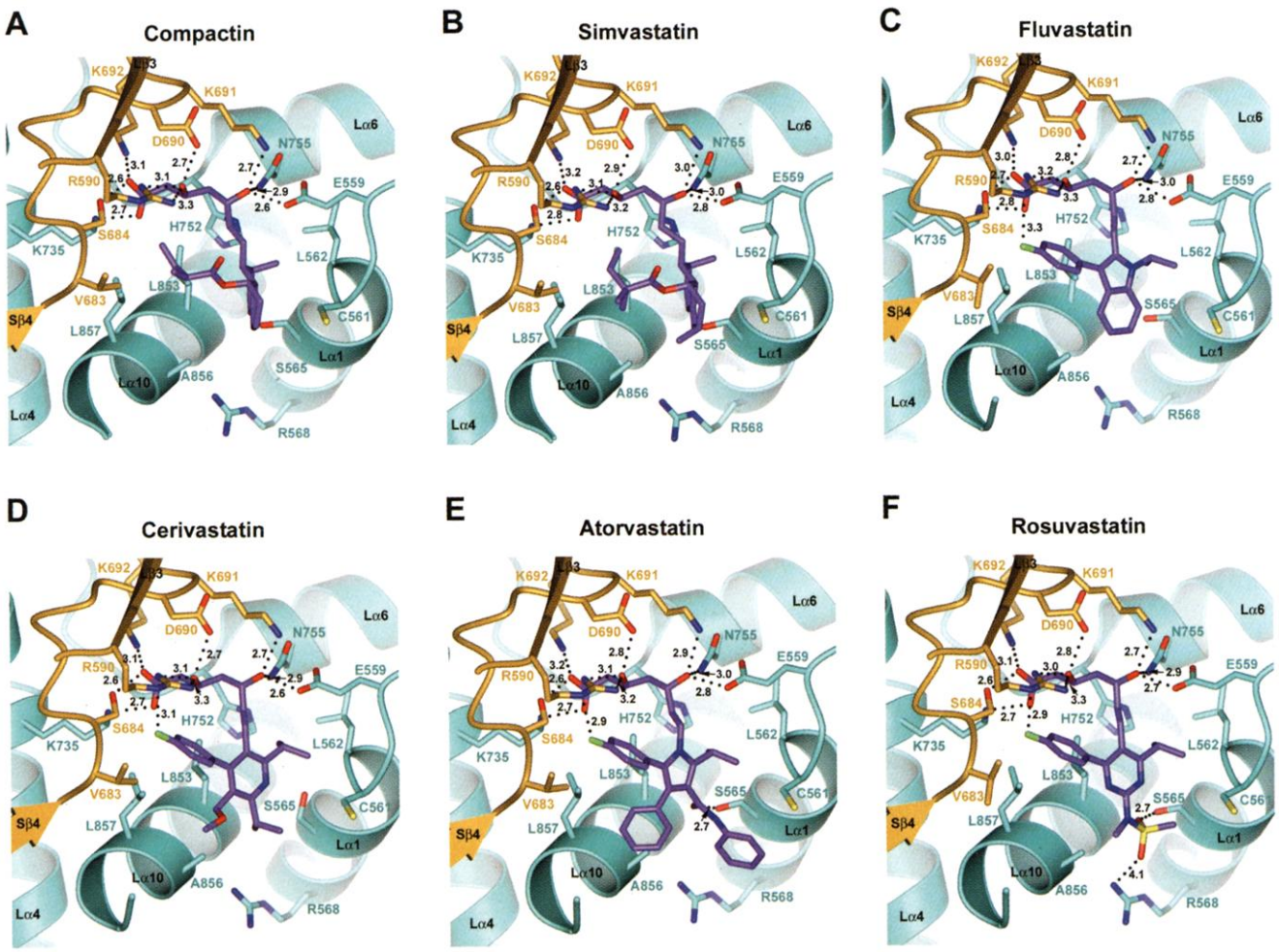

Fig. 4. Mode of binding of compactin (**A**), simvastatin (**B**), fluvastatin (**C**), cerivastatin (**D**), atorvastatin (**E**), and rosuvastatin (**F**) to human HMGR. Interactions between the HMG moieties of the statins and the protein are mostly ionic or polar. They are similar for all inhibitors and are indicated by the dotted lines. Numbers next to the lines indicate distances in Å (*13*). The rigid hydrophobic groups of the statins are situated in a shallow groove between helices Lα1 and Lα10. Additional interactions between Arg^{590} and the fluorophenyl group are present in the type 2 statins (C, D, E, F). Atorvastatin and rosuvastatin form a hydrogen bond between Ser^{565} and a carbonyl oxygen atom (atorvastatin) (E) or a sulfone oxygen atom (rosuvastatin) (F).

Table 1. Data collection and refinement statistics. Constants a, b, and c are in Å; β is in degrees. *n*, number; Rmsd, root mean square deviation.

Crystal	Compactin	Simvastatin	Fluvastatin	Cerivastatin	Atorvastatin	Rosuvastatin
Cell constants	a = 73.8 b = 173.0 c = 75.2 β = 118.4	a = 74.6 b = 172.8 c = 80.0 β = 117.6	a = 74.8 b = 175.1 c = 74.8 β=118.3	a = 74.6 b = 173.0 c = 80.2 β = 117.4	a = 74.6 b = 172.7 c = 80.0 β = 117.7	a = 74.4 b = 172.5 c = 80.0 β = 117.4
Crystals (*n*)	1	1	1	1	1	2
Resolution (Å)	43.1 to 2.10	43.4 to 2.33	43.8 to 2.30	43.5 to 2.26	43.4 to 2.22	43.3 to 2.10
Unique reflections (*n*)	89,377	73,699	73,193	80,409	86,963	101,733
Redundancy	2.4	3.9	3.6	4.2	3.7	5.0
Completeness (%)	92.7	96.4	97.6	96.0	98.6	97.6
R_{sym} (%)*	5.4	6.4	10.0	4.7	3.8	7.2
$\langle I/\sigma I \rangle$	14.8	20.7	11.8	28.7	30.8	21.1
Protein atoms (*n*)	11,565	11,750	11,398	11,938	11,772	11,764
Water molecules (*n*)	287	176	199	186	225	182
Heterogen atoms (*n*)	170	259	201	294	299	213
Rmsd bond lengths (Å)	0.011	0.009	0.009	0.010	0.011	0.087
Rmsd bond angles (°)	1.5	1.3	1.4	1.4	1.4	1.7
Average B factor (Å^2)	36.8	60.4	28.3	55.1	52.7	55.4
$R_{working}$ (%)†	19.1	22.2	18.6	22.1	21.2	21.9
R_{free} (%)‡	22.3	24.8	21.4	23.7	23.5	23.9
PDB accession no.	1HW8	1HW9	1HWI	1HWJ	1HWK	1HWL

*$R_{merge} = \Sigma|(I_{hkl}) - \langle I \rangle| / \Sigma (I_{hkl})$, where I_{hkl} is the integrated intensity of a given reflection. †$R = (\Sigma|F_{obs} - F_{calc}|) / (\Sigma F_{obs})$, where F_{obs} and F_{calc} are observed and calculated structure factors, respectively; no $I/\sigma I$ cutoff was used in the refinement. ‡For each crystal, about 2000 reflections were excluded from the refinement to calculate R_{free}.

strate complex (Fig. 2). Several polar interactions are formed between the HMG-moieties and residues that are located in the cis loop (Ser^{684}, Asp^{690}, Lys^{691}, Lys^{692}). Lys^{691} also participates in a hydrogen-bonding network with Glu^{559}, Asp^{767} and the O5-hydroxyl of the statins. The terminal carboxylate of the HMG moiety forms a salt bridge to Lys^{735}. The large number of hydrogen bonds and ion pairs results in charge and shape complementarity between the protein and the HMG-like moiety of the statins. Identical bonding interactions are observed between the protein and HMG and presumably also with the reaction product mevalonate (Fig. 2A). Because mevalonate is released from the active site, it is likely that not all of its interactions with the protein are stabilizing. These observations suggest that the hydrophobic groups of the inhibitors are predominately responsible for the nanomolar K_i values; they may also change the context of the HMG-like polar interactions such that the ion pairs contribute favorably to the binding of statins.

Hydrophobic side chains of the enzyme involving residues Leu^{562}, Val^{683}, Leu^{853}, Ala^{856}, and Leu^{857} participate in van der Waals contacts with the statins. The surface complementarity between HMGR and the hydrophobic ring structures of the statins is present in all enzyme-inhibitor complexes, despite the structural diversity of these compounds. This is possible because the type 1 and type 2 statins adopt different conformations that allow their hydrophobic groups to maximize contacts with the hydrophobic pocket on the protein (Fig. 4). Functionally, the methylethyl group attached to the central ring of the type 2 statins replaces the decalin of the type 1 statins. The butyryl group of the type 1 statins occupies a region similar to the fluorophenyl group present in the type 2 inhibitors.

A comparison between the six complex structures illustrates subtle differences in their modes of binding. Rosuvastatin has the greatest number of bonding interactions with HMGR (Fig. 4F). In addition to numerous contacts present in other statin-HMGR complex structures, a polar interaction between the Arg^{568} side chain and the electronegative sulfone group is unique to rosuvastatin. Present only in atorvastatin and rosuvastatin are hydrogen bonds between Ser^{565} and either a carbonyl oxygen atom (atorvastatin) or a sulfone oxygen atom (rosuvastatin) (Fig. 4, E and F). The fluorophenyl groups of type 2 statins are one of the main features distinguishing type 2 from the type 1 statins. Here, the guanidinium group of Arg^{590} stacks on the fluorophenyl group, and polar interactions between the arginine ε nitrogen atoms and the fluorine atoms are observed. No differences between the type 1 statins compactin and simvastatin are apparent (Fig. 4, A and B). With the exception of the larger atorvastatin, the solvent-accessible areas of unbound or bound statins and the buried areas upon statin binding to HMGR are similar for all inhibitors (*13*).

In summary, these studies reveal how statins bind to and inhibit their target, human HMGR. The bulky, hydrophobic compounds of statins occupy the HMG-binding pocket and part of the binding surface for CoA. Thus, access of the substrate HMG-CoA to HMGR is blocked when statins are bound. The tight binding of statins is probably due to the large number of van der Waals interactions between inhibitors and with HMGR. The structurally diverse, rigid hydrophobic groups of the statins are accommodated in a shallow non-polar groove that is present only when COOH-terminal residues of HMGR are disordered. Although the statins that are currently available or in late-stage development excel in curtailing the biosynthesis of mevalonate, the precursor of cholesterol, it is possible that the visualization of statin bound to HMGR will assist in the development of even better inhibitors. In particular, it should be noted that the nicotinamide-binding site of HMGR is not occupied by statin inhibitors and that the covalent attachment of a nicotinamide-like moiety to statins might improve their potency.

References and Notes

1. D. A. Eisenberg, *Am. J. Med.* **104**, 2S (1998).
2. Y. Kureishi *et al.*, *Nature Med.* **6**, 1004 (2000).
3. G. Mundy *et al.*, *Science* **286**, 1946 (1999).
4. J. Davignon, R. Laaksonen, *Curr. Opin. Lipidol.* **10**, 543 (1999).
5. A. Corsini, F. M. Maggi, A. L. Catapano, *Pharmacol. Res.* **31**, 9 (1995).
6. A. Endo, M. Kuroda, K. Tanzawa, *FEBS Lett.* **72**, 323 (1976).
7. K. M. Bischoff, V. W. Rodwell, *Biochem. Med. Metab. Biol.* **48**, 149 (1992).
8. E. S. Istvan, M. Palnitkar, S. K. Buchanan, J. Deisenhofer, *EMBO J.* **19**, 819 (2000).
9. E. S. Istvan, J. Deisenhofer, *Biochim. Biophys. Acta* **1529**, 9 (2000).
10. The catalytic portion of human HMGR was purified as described (*8*). Concentrated stock solutions of the inhibitors were prepared in methanol and added to the protein in three- or fourfold molar excess. Simvastatin, fluvastatin, cerivastatin, atorvastatin, and rosuvastatin were received from AstraZeneca and were in their active hydroxy-acid form. Compactin was purchased from Sigma and activated by converting the lactone form to the sodium salt with NaOH as described (*14*). After a 6 to 24 hour incubation of protein with inhibitor at 4°C, batch crystallization trials at 21°C were set up. Crystals were grown at a protein concentration of 3 to 5 mg/ml and in solutions containing 12 to 15 % [weight/volume (w/v)] polyethylene glycol (PEG) 4000, 0.15 to 0.2 M ammonium acetate, 25 mM Na-Hepes (pH 7.5), 50 mM

dithiothreitol (DTT), 10 mM adenosine diphosphate (ADP), and 10% glycerol. Crystallization was initiated by the addition of microseeds, prepared from substrate crystals, after 14 to 20 hours. Plate-like crystals grew in about 10 days. The crystals were harvested in solutions containing 20% (w/v) PEG 4000, 0.3 M ammonium acetate, 25 mM Na-Hepes (pH 7.5), 50 mM DTT, 10 mM ADP and 10% glycerol. For cryoprotection, the crystals were transferred to solutions containing increasing glycerol (15, 20, and 25%) for about 1 min each and flash-cooled in liquid propane. Initial data for a rosuvastatin complex structure to a resolution of 2.4 Å were collected at beamline 5.0.2 of the Advanced Light Source (ALS) synchrotron, which is supported by the Director, Office of Science, Office of Basic Energy Sciences, Materials Sciences Division of the U.S. Department of Energy under Contract No. DE-AC03-76SF00098 at Lawrence Berkeley National Laboratory. Data for the other inhibitor complexes and higher resolution data for the rosuvastatin complex were collected at beamline F1 at the Cornell High Energy Synchrotron Source (CHESS), which is supported by the National Science Foundation under award DMR-9311772, using the Macromolecular Diffraction at CHESS (MacCHESS) facility, which is supported by award RR-01646 from the National Institutes of Health. Data reduction and processing were carried out with the HKL package (*15*). Because the low-resolution data for the rosuvastatin complex crystal was incomplete for the data collected at CHESS, the reduced data were merged with the reduced data collected at ALS during scaling. All crystals have the symmetry of space group $P2_1$ and contain four HMGR monomers in each asymmetric unit, although two different crystal forms were observed (Table 1). The protein portion of the structure of human HMGR in complex with HMG, CoA, and $NADP^+$ [Protein Data Bank (PDB) code 1dqa] was used as the starting model for the refinement. Initially, the inhibitor molecules were placed into F_o-F_c electron-density maps. Subsequently, their positions were modified by consulting σ_A weighted $2F_o$-F_c maps (*16*) and simulated-annealing omit maps (*17*). The models were built using the program O (*18*) and refined with CNS (*19*). Bulk solvent, overall aniosotropic B-factor scaling, and noncrystallographic symmetry restraints were applied throughout the refinement process. For each of the six HMGR-statin complexes, the electron-density maps were excellent for all four statin molecules bound to the four crystallographically independent monomers. Additionally, poor electron density was located close to residues Y479 and F629 (*20*) and was interpreted as ADP. The positions of the ADP molecules resemble the positions of the adenosine moieties of the substrates CoA or NADPH. ADP was bound only to some of the CoA or NADPH binding sites and the number of ADP molecules is different for the six structures.

11. C. M. Lawrence, V. W. Rodwell, C. V. Stauffacher, *Science* **268**, 1758 (1995).
12. L. Tabernero, D. A. Bochar, V. W. Rodwell, C. V. Stauffacher, *Proc. Natl. Acad. Sci. U.S.A.* **96**, 7167 (1999).
13. All calculations on accessible or buried surface areas for the statins or the protein, as well as distance information between specific groups, represent averages for the four crystallographically independent statin molecules observed in each complex structure. The surface accessible areas for the unbound statins, the bound statins, and the buried surface areas upon statin binding to HMGR, respectively, are as follows: compactin 670 Å^2, 100 Å^2, 880 Å^2; simvastatin 670 Å^2, 110 Å^2, 880 Å^2; fluvastatin 660 Å^2, 80 Å^2, 870 Å^2; cerivastatin 720 Å^2, 100 Å^2, 880 Å^2; atorvastatin 840 Å^2, 150 Å^2, 1060 Å^2; and rosuvastatin 710 Å^2, 130 Å^2, 880 Å^2.
14. M. S. Brown, J. R. Faust, J. L. Goldstein, *J. Biol. Chem.* **253**, 1121 (1978).
15. Z. Otwinowski, W. Minor, *Methods Enzymol.* **276**, 306 (1997).
16. A. Hodel, S.-H. Kim, A. T. Brünger, *Acta Crystallogr. A* **48**, 851 (1992).
17. R. J. Read, *Acta Crystallogr. A* **1986**, 140 (1986).
18. T. A. Jones, J. Y. Zou, S. W. Cowan, M. Kjeldgaard, *Acta Crystallogr. A* **47**, 110 (1991).
19. A. T. Brünger *et al.*, *Acta Crystallogr. D* **54**, 905 (1998).
20. Single-letter abbreviations for the amino acid residues are as follows: A, Ala; C, Cys; D, Asp; E, Glu; F, Phe; G, Gly; H, His; I, Ile; K, Lys; L, Leu; M, Met; N, Asn; P, Pro; Q, Gln; R, Arg; S, Ser; T, Thr; V, Val; W, Trp; and Y, Tyr.
21. G. A. Holdgate *et al.*, in preparation.
22. R. M. Esnouf, *Acta Crystallogr. D* **55**, 938 (1999).
23. L. Esser, personal communication.
24. Persistence of Vision Ray Tracer v.3.02, Copyright 1997, POV-Team. www.povray.org

25. We thank AstraZeneca for providing simvastatin, fluvastatin, cerivastatin, atorvastatin, and rosuvastatin and for stimulating discussions; S. Jeong for converting compactin to the active sodium salt form; the personnel at ALS beamline 5-1 and CHESS beamline F1 for their assistance in data collection; and C. A. Brautigam for critical reading of the manuscript. The coordinates are available from the PDB (accession numbers are indicated in Table 1).

26 January 2001; accepted 3 April 2001

Control of a Genetic Regulatory Network by a Selector Gene

Kirsten A. Guss,* Craig E. Nelson,* Angela Hudson, Mary Ellen Kraus, Sean B. Carroll†

The formation of many complex structures is controlled by a special class of transcription factors encoded by selector genes. It is shown that SCALLOPED, the DNA binding component of the selector protein complex for the *Drosophila* wing field, binds to and directly regulates the cis-regulatory elements of many individual target genes within the genetic regulatory network controlling wing development. Furthermore, combinations of binding sites for SCALLOPED and transcriptional effectors of signaling pathways are necessary and sufficient to specify wing-specific responses to different signaling pathways. The obligate integration of selector and signaling protein inputs on cis-regulatory DNA may be a general mechanism by which selector proteins control extensive genetic regulatory networks during development.

The concept of the morphogenetic field, a discrete set of cells in the embryo that gives rise to a particular structure, has held great importance in experimental embryology (*1*). The discovery of genes whose products control the formation and identity of various fields, dubbed "selector genes" (*2*), has enabled the recognition and redefinition of fields as discrete territories of selector gene activity (*3*). Although the term has been used somewhat liberally, two kinds of selector genes have been of central interest to understanding the development of embryonic fields. These include the *Hox* genes, whose products differentiate the identity of homologous fields, and field-specific selector genes such as *eyeless* (*4*), *Distal-less* (*5*), and *vestigial-scalloped* (*vg-sd*) (*6–8*), whose products have the unique property of directing the formation of entire complex structures. The mechanisms by which field-specific selector proteins direct the development of these structures are not well understood. In principle, selector proteins could directly regulate the expression of only a few genes, thus exerting much of their effect indirectly, or they may regulate the transcription of many genes distributed throughout genetic regulatory networks.

In the *Drosophila* wing imaginal disc, the VG-SD selector protein complex regulates wing formation and identity (*7*, *8*). SD is a TEA-domain protein (*9*) that binds to DNA in a sequence-specific manner (*7*), whereas VG, a novel nuclear protein (*10*), functions as a trans-activator (*11*). To determine whether direct regulation by SD is widely required for gene expression in the wing field, we analyzed the regulation of several genes that represent different nodes in the wing genetic regulatory network and that control the development of different wing pattern elements (Fig. 1A). We focused in particular on genes for which cis-regulatory elements that control expression in the wing imaginal disc have been isolated, including *cut* (*12*), *spalt* (*sal*) (*13*), and *vg* (*6*).

We first tested whether *sd* gene function was required for the expression of various genes in the wing field. We generated mitotic clones of cells homozygous for a strong hypomorphic allele of *sd* and assessed the expression of gene products or reporter genes within these clones (*14*). Reduction of *sd* function reduced or eliminated the expression of the CUT (Fig. 1, B and F) and WINGLESS (WG) (Fig. 1, C and G) proteins and of reporter genes under the control of the *sal* 10.2-kb (Fig. 1, D and H) and the *vg* quadrant (Fig. 1, E and I) enhancers,

Howard Hughes Medical Institute and Laboratory of Molecular Biology, University of Wisconsin, Madison, WI 53706, USA.

*These authors contributed equally to this work.
†To whom correspondence should be addressed. E-mail: sbcarrol@facstaff.wisc.edu